



**HAL**  
open science

## Plasma polymer for enhancing adhesion bonds of metal/elastomer assembly

Marisol Ji, Lazhar Benyahia, Fabienne Poncin-Epaillard

► **To cite this version:**

Marisol Ji, Lazhar Benyahia, Fabienne Poncin-Epaillard. Plasma polymer for enhancing adhesion bonds of metal/elastomer assembly. *Plasma Processes and Polymers*, 2021, 18 (9), pp.2100035. 10.1002/ppap.202100035 . hal-03367437

**HAL Id: hal-03367437**

**<https://hal.science/hal-03367437>**

Submitted on 6 Oct 2021

**HAL** is a multi-disciplinary open access archive for the deposit and dissemination of scientific research documents, whether they are published or not. The documents may come from teaching and research institutions in France or abroad, or from public or private research centers.

L'archive ouverte pluridisciplinaire **HAL**, est destinée au dépôt et à la diffusion de documents scientifiques de niveau recherche, publiés ou non, émanant des établissements d'enseignement et de recherche français ou étrangers, des laboratoires publics ou privés.

# Plasma polymer for enhancing adhesion bonds of metal/elastomer assembly

Marisol Ji<sup>1)</sup>, Lazhar Benyahia<sup>1)</sup>, Fabienne Poncin-Epaillard<sup>1\*)</sup>

1) Institut des Molécules et Matériaux du Mans, Le Mans Université – CNRS n°6283, Avenue Olivier Messiaen, 72085 Le Mans, France

\*) Corresponding author, Fabienne.poncin-epaillard@univ-lemans.fr

**Keywords:** plasma polymerization, acetylene, acrylic acid, maleic anhydride, FTIR, XPS, multilayers.

## Abstract:

Four model plasma coatings obtained with selected parameters and precursors (acetylene, acrylic acid and maleic anhydride) were developed for the preparation of adhesive joints of metal / elastomer assembly. One of these layers, PW, is thin and highly functionalized while another (CW) coated with the same thickness is less functionalized but crosslinked. The two other layers (CW x 2, CW + PW), twice as thick compared to PW and CW, show the same chemical criteria. The adhesion strength of prepared assemblies is increasing but mostly depends on the precursor type. Moreover, such model layers allow to study the adhesion mechanism between the metal and the elastomer. The thermodynamic adhesion, i.e. surface energy closer to the elastomer one appears to prevail.

## 1. Introduction

Plasma-enhanced chemical vapor deposition (PECVD) has been used to coat plasma-polymerized (pp) films on various substrates, either metal or polymers. The properties of such a coating can be adjusted by optimizing deposition parameters including monomer type (hydrophobic or hydrophilic), duration, power, duty cycle and various others depending on the plasma chamber characteristics.<sup>[1-7]</sup> Single layers but also multilayers with chemical composition gradient in thickness can be also prepared with the plasma technology and this type of thin film

process is credited with providing outstanding properties such as the adhesion between the plasma polymer and the substrate.<sup>[8,9]</sup> Furthermore, the interfacial adhesion between each individual layer enhances the tribology properties of assemblies inhibiting cracking and delamination.<sup>[10]</sup> And the barrier properties of the multilayers are also increasing since such material avoids polymeric chain reptation and dissolution of one layer components into the closest layer.<sup>[11,12]</sup> The multilayer plasma coating could be applied to a wide range of precursors and various substrates, polymers or metals.<sup>[13-17]</sup> But, in our knowledge, little attention was paid to the effect of their respective surface and bulk chemical functionality, their thickness and their crosslinking compared to a single layer originated from the same precursor.

The pulsed plasma polymerization of three different precursors (acetylene - Ac, acrylic acid - AA; maleic anhydride - MA) was shown to be a promising method and the chemical retention depends on the plasma chamber.<sup>[3,4,18-23]</sup> Their corresponding plasma polymers adhered on various substrates, mostly metallic ones for the pp-Ac<sup>[24-26]</sup> and polymeric ones for the two other precursors.<sup>[27-28]</sup> So here, the study was extended to other plasma parameters alone or combined (pulsed or continuous wave at different discharge powers, durations...) in order to synthesize the four model layers and to compare their efficiency for the adhesive vulcanization allowed the cohesion of metal elastomer assembly..

The plasma synthesis of these layers differs in order to vary their chemical composition at constant and similar thickness about few 10 or 100 nm depending on precursor chemistry. Pulsed wave (PW) films are carried out under conditions less degrading and preserving the chemical groups of each precursor. This model should promote the chemical adhesion. Continuous wave coatings (CW) are opposite to the previous ones with less reactive group retention, namely because of a high fragmentation of the precursors by electronic impact under a continuous discharge. The third experiment (CW x 2) plays on the thickness of the film, i.e on duration without providing targeted chemical functionality (no retention). This path should be only in favor of the interdiffusion of macromolecular chains. The last experiment (CW + PW) is intermediate to the other methods. A thick layer about several 10 nm is first deposited on the substrate under continuous wave; then at the extreme surface the chemical functionalization is provided by the deposition in pulsed wave under optimal retention conditions. This experimental path should combine the effects of chemical anchoring and interdiffusion with a chemically controlled surface and a relatively thick film to facilitate the creation of an interphase during further adhesive

vulcanization. The validation of these model layers is illustrated by measuring the mechanical strength of two assemblies (aluminum - poly(acrylonitrile butadiene) rubber (NBR) and stainless steel - fluoroelastomer (FKM)).

## 2. Materials and methods

### 2.1 Materials and plasma deposition, assembly preparation

The organic precursors used without any further purification were: gaseous acetylene (AirLiquid, purity 99.95%) and liquid acrylic acid (Sigma-Aldrich, purity 99%) which was filled into a quartz tube connected to the chamber and vaporized due to the low pressure. The used solid maleic anhydride (Sigma-Aldrich, purity 99%) was filled in the quartz tube heating at 52 °C and vaporized in gas line heated at 75 °C. The chosen elastomers were poly(acrylonitrile butadiene) rubber (NBR), fluoroelastomer (FKM) respectively provided respectively by Safran and EFJM societies.

Plasma polymerization was performed in a capacitively coupled radio-frequency (RF, 13.56 MHz) plasma reactor. The low pressure was maintained thanks to a turbomolecular pump (Alcatel ATP-80) coupled to a primary rotary pump. Typical residual pressures were maintained between  $10^{-5}$  and  $10^{-4}$  mbar, while the working pressure was kept around  $10^{-2}$  mbar and measured by a wide range capacitive-penning pressure gauge (Alcatel ACC 1009). The glow discharge was sustained between two parallel electrodes separated by a fixed distance of 12 cm, and powered with a Caesar RF generator (Advanced Energy), with powers ranging from 5 to 100 W. Reflected power was kept to a minimum thanks to a RF Navio matchbox (Advanced Energy). Plasma discharges were sustained in the different atmospheres: acetylene at different flow rates ( $Q$  from 10 to 40 sccm), and for vapours of pure AA or MA. For the latter, as their flow rates were not controlled, their content in the chamber was fixed with a constant working pressure of  $1.0 \cdot 10^{-2}$  mbar. Typically, the plasma parameters for the different precursors and model layers based on our previous study<sup>[6]</sup> were described in Table 1:

Table 1: Plasma parameters applied to the different precursor depending on the model layer

	PW	CW	CW x 2	CW + PW
pp-Ac $P = 50$ W, $Q = 40$ sccm	$f = 7$ kHz, $d.c = 11$ % , $t = 60$ min	$t = 13$ min	$t = 26$ min	CW : $t = 13$ min PW : $f = 7$ kHz, $d.c = 11$ % , $t = 60$ min

pp-AA $P = 10 \text{ W}, p = 0.01 \text{ mbar}$	$f = 5 \text{ kHz}, d.c = 8 \%,$ $t = 5 \text{ min}$	$t = 2 \text{ min}$	$t = 4 \text{ min}$	CW : $t = 2 \text{ min}$
				PW : $f = 5 \text{ kHz}, d.c = 8 \%, t = 5 \text{ min}$
pp-MA $P = 10 \text{ W}, p = 0.01 \text{ mbar}$	$f = 5 \text{ kHz}, d.c = 8 \%,$ $t = 20 \text{ min}$	$t = 14.5 \text{ min}$	$t = 29 \text{ min}$	CW : $t = 14.5 \text{ min}$
				PW : $f = 5 \text{ kHz}, d.c = 8 \%, t = 20 \text{ min}$

The assembly was prepared with the elastomer (thickness =  $3.5 \pm 0.3 \text{ mm}$ , diameter = 8.0 mm) inserted between two metallic disks (aluminum or stainless steel respectively for NBR and FKM assemblies, diameter = 8 mm, contact area =  $5.03 \cdot 10^{-5} \text{ m}^2$ ) cleaned with acetone in ultrasonic bath and layered with the plasma coating. Then, the vulcanization was taken place under shear (0.1 strain%) with a frequency of 10 rad/s, compression applied with 1.5 Kg (14.71 N) strength at 180 °C and 160 °C for respectively FKM and NBR during 15 min.

## 2.2 Characterization

Each model plasma layer was characterized by FTIR, XPS spectroscopies and wettability measurements as described here.

### *FTIR spectroscopy*

Chemical composition of the plasma polymers (pp-Ac, pp-AA and pp-MA) coated on transparent KBr pellets was measured via a Bruker Vertex 70 v spectrometer with  $2 \text{ cm}^{-1}$  resolution in the range  $4000 - 400 \text{ cm}^{-1}$ , 40 scans were recorded under vacuum. The FTIR spectra were done 10 min after the sample deposition and the background spectrum was subtracted. Spectral data were treated with Opus software for baseline correction and  $\text{CO}_2/\text{H}_2\text{O}$  subtraction.

### *XPS spectroscopy*

The plasma coating on Si/SiO<sub>2</sub> wafers were analyzed by X-Ray Photoelectron Spectroscopy (XPS) instrument (Kratos Axis Nova, UK, Institut des Matériaux de Nantes, France) with the monochromatic Al K $\alpha$  beam, whose energy is equal to 1486.7 eV, at the electron emission angle of 90 ° relative to the sample surface. The pass energies for survey spectra were 80 eV (increment = 0.5 eV) and 20 eV (increment = 0.1 eV) for high resolution. The charging effect was corrected with C-C binding energy as reference at 285.0 eV and the background subtraction was performed.

The full width at half-maximum for the Gaussian peaks was maintained as a constant value for all components around 1.4 eV depending on the layer type. The resolution fitting accuracy was 5%.

#### *Wettability and surface free energy*

The wettability of the plasma layers on silica substrate was tested by means of a goniometer with 3  $\mu\text{l}$  high purity water drops (MilliQWater System, resistivity  $18 \text{ M}\Omega\cdot\text{cm}^{-1}$ ) and diiodomethane drops (Sigma-Aldrich France,  $\geq 99 \%$ ). Measurements were run on both sides of the drop and were averaged of five experiments. The surface energy was calculated by the Owens–Wendt method.<sup>[29]</sup>

#### *Layer thickness measurement*

The thickness measure of the different layers coated on Si/SiO<sub>2</sub> wafer was performed with an AFM machine (Bruker Innova). Before the deposition, the substrate was partially masked. After the plasma process, the mask was removed and the level difference corresponds to the thickness of the thin film.  $50 \times 50 \mu\text{m}^2$  areas of at least 5 different samples were scanned in tapping mode at ambient air. The film thicknesses were determined using Gwyddion software (2.50).

#### *Decohesion of the assembly*

The strength needed for assembly decohesion was measured with ZwickRoell Z0101 with 500 N of test load Fmax at constant rate (0.1 mm / min). The applied strength on the overall contact area between the metallic substrate and the elastomer was measured versus the shift, and values of stress and deformation were then extracted. Here, only the yield stress, i.e. the maximum value of stress due to the beginning of the assembly rupture is discussed.

### **3. Results and discussion**

#### **3.1 Comparative study of plasma polymerization kinetics of the three precursors under continuous or pulsed wave**

Before preparing and characterizing the different layers PW, CW, CW x 2 and PW + CW with equivalent thickness, kinetics study of each type of precursor and discharge was run regardless

of the chosen reaction pattern. In order to limit the number of experiments, only the overall duration is studied while the other plasma parameters (power, flow rate and pressure) are constant.

Table 2: Dependence of the different coating rates ( $\text{nm}\cdot\text{min}^{-1}$ ) on discharge wave and precursor

	PW	CW
pp-Ac	$1.08 \pm 0.03$	$5.2 \pm 0.4$
pp-AA	$1.25 \pm 0.17$	$5.4 \pm 0.3$
pp-MA	$1.38 \pm 0.18$	$2.4 \pm 0.1$

The Fig. S1 shows an almost linear dependence in the thickness whatever the precursor chemical nature and the discharge; the corresponding plasma polymerization kinetics are close to the first order of reaction meaning that the density of reactive plasma species does not vary with time.<sup>[1]</sup> Moreover, only pp-Ac and pp-AA growths with continuous plasma phase are faster ( $5.20 \text{ nm}\cdot\text{min}^{-1}$ ). Indeed, as noticed in Table 2 in CW discharge, acrylic acid therefore polymerizes little faster than acetylene but for both faster than maleic anhydride. The deposition conditions differ between pp-Ac and two other polymers. But, despite a discharge power 5 times higher inducing a more intense electron bombardment, Ac kinetics is little slower ( $5.2 \text{ nm}\cdot\text{min}^{-1}$ ), probably due to higher triple bond scission and ionization energies, respectively 11.40 eV and 10 eV, compared to AA ones (ionization energy = 10.6 eV and double bond scission energy = 6.35 eV).<sup>[30]</sup> Moreover, if the monomer radicals are stabilized in the plasma phase as shown for the styrene<sup>[31]</sup> or AA<sup>[1]</sup> polymerization, the respective deposition rate is higher or at least close to that one of alkyne compound.

The growth of the pp-MA is almost twice lower whatever the discharge frequency and should be interpreted as evidence of degradation during deposition. This difference between the pulsed and continuous discharges can be explained by more or less intense bombardments of electrons, ions and photons in both gas and solid phase but also by an indirect heating of the substrate generated by these bombardments.<sup>[32,33]</sup> The appearance of a greater number of radicals in the films deposited in continuous wave could also affect the growth. These phenomena occurring at the surface, probably more marked with MA induce instability of the growing layer, or even its degradation as observed by Manakhov *et al.*,<sup>[34]</sup> showing that for the same discharge power and the same injection rate, the deposition rate is lower in CW discharge. Indeed, this low deposition rate also observed in<sup>[35]</sup> was explained by the precursor degradation forming stable degraded product as  $\text{CO}_2$ .<sup>[6,7,36,37]</sup>

From this short kinetics study, plasma parameters were defined for the PW, CW, CW x 2 and CW + PW layers as described in Table 1. Such plasma parameters lead to coatings whose thicknesses of pp-Ac vary from  $59.3 \pm 3.1$  to  $107 \pm 12.3$  nm (Fig. 1). The thickness of the pp-AA layers doubles for the CW x 2 and CW + PW strategies ranging from  $7.4 \pm 1.2$  to  $17.6 \pm 2$  nm. Finally, the thickness of the pp-MA coatings varies from  $30.2 \pm 4.6$  to  $67.0 \text{ nm} \pm 7.7$  nm.

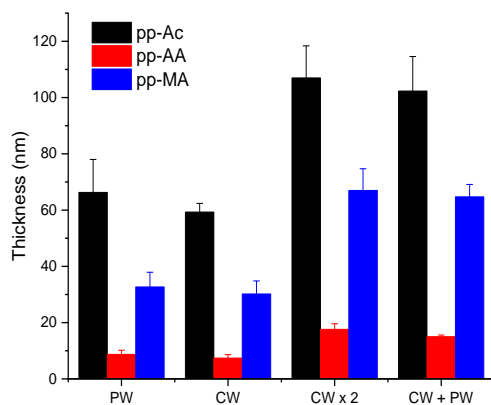


Fig. 1: Thickness of PW, CW, CW x 2 and CW + PW layers (pp-Ac:  $P = 50$  W,  $Q = 40$  sccm, pp-AA and pp-MA:  $P = 10$  W,  $p = 0.01$  mbar)

For each precursor, two sets of layers were obtained. The first one (PW, CW) of low thickness (pp-AC:  $\approx 63$  nm, pp-AA:  $\approx 8$  nm, pp-MA  $\approx 31$  nm) and a second series (CW x 2, CW + PW) of almost double thickness (pp-AC:  $\approx 105$  nm, pp-AA:  $\approx 16$  nm, pp-MA  $\approx 65$  nm). In each set, one layer (PW and CW + PW) has its chemical surface functionality preserved.

### 3.2 Comparative characterization of physicochemical properties of the different model layers

Various characterizations with different analyze depths were applied in order to determine if the PW, CW + PW bear chemical groups of each precursor compared to the thicker layers CW and CW x 2.

*Bulk chemical characterization issued from FTIR spectroscopy*

The analysis of the FTIR spectra of the different model films were carried out (Fig. 2). followed by the interpretation of the ratio of relative band intensity given in Fig. 3. Details on each vibration band assignment were fully described in Table S1 (supporting information file).

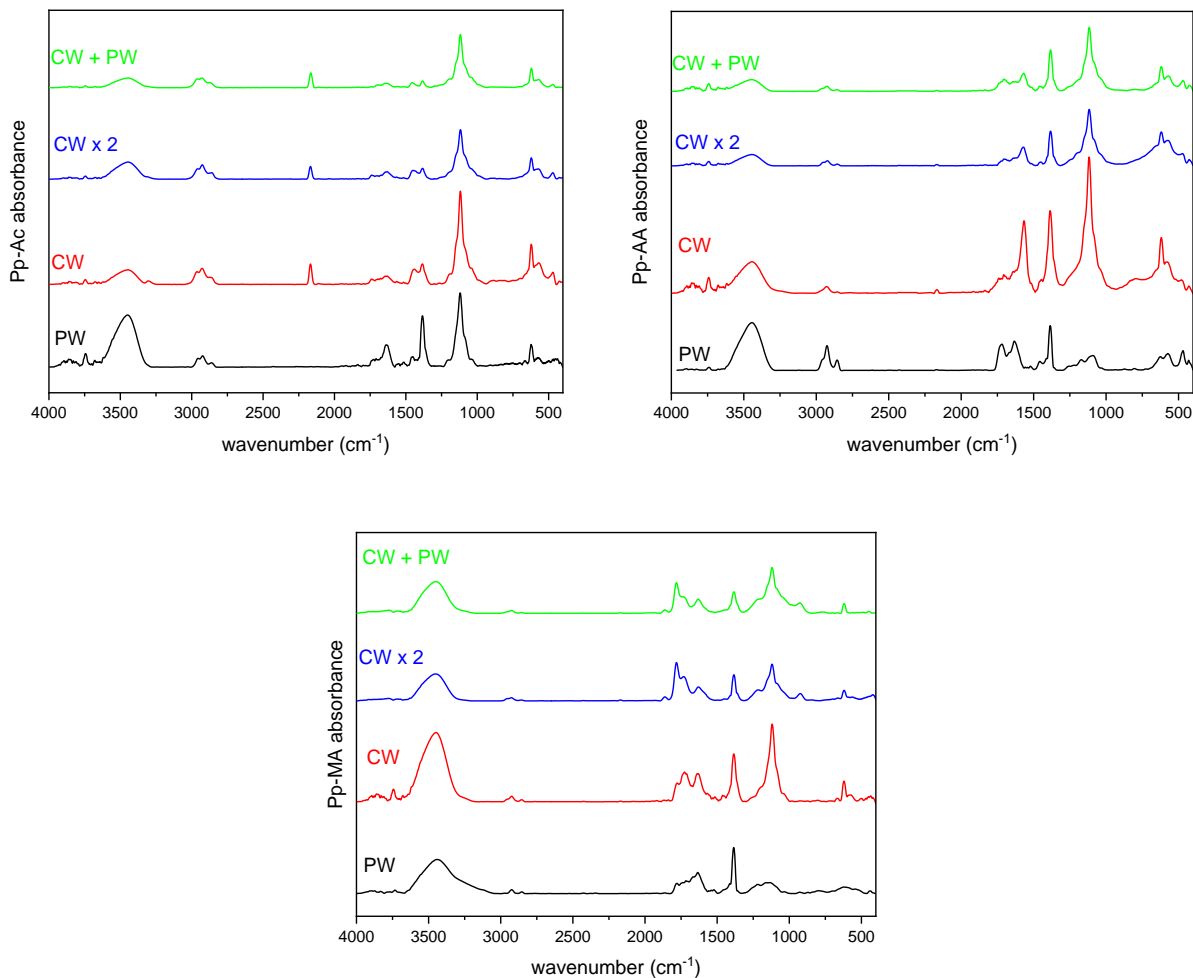


Fig. 2: FTIR spectra of PW, CW, CW x 2 and CW + PW layers (pp-Ac:  $P = 50$  W,  $Q = 40$  sccm, pp-AA and pp-MA:  $P = 10$  W,  $p = 0.01$  mbar)

Compared to PW pp-Ac spectrum (Fig. 2), the three other spectra of pp-Ac prepared in a continuous wave including the CW + PW show the decrease of O-H band at  $3450\text{ cm}^{-1}$ , C=C bond elongation band at  $1645\text{ cm}^{-1}$ ,  $\text{CH}_2$  and  $\text{CH}_3$  stretch band between  $1320$  and  $1484\text{ cm}^{-1}$  and the appearance of a new band at  $2170\text{ cm}^{-1}$  assigned to the disubstituted C-C alkyne.<sup>[38,39]</sup> This is significant of a high fragmentation of plasma species produced in continuous wave leading to a more crosslinked and less oxidized coating. The appearance of the disubstituted C-C alkyne band indicates that the acetylene fragments are quite complex and their recombination does not

specifically lead to a saturated network. It must be noticed that the pp-Ac oxidation corresponds to the dangling radicals formed during the plasma polymerization. Moreover, such oxidation may also be assigned to oxygen / water desorption from the chamber walls or to acetone plasma fragmentation. Indeed, this molecule is added in the acetylene bottle for safe storage and was interfering in some surface modifications.<sup>[40]</sup> The observed similarity of CW + PW and CW spectrum is explained by a lack of FTIR sensitivity toward the upper thin layer as the analysis is recorded using the transmission mode. The three spectra of pp-AA prepared in one or two steps, compared to that one of PW show a decrease of OH vibration band at  $3446\text{ cm}^{-1}$ , of  $\text{CH}_2$  and  $\text{CH}_3$  stretch band around  $2960 - 2860\text{ cm}^{-1}$ . However, the most remarkable feature of these spectra is the increase of C-C stretch band at  $1100\text{ cm}^{-1}$  and the appearance of a new band at  $1560\text{ cm}^{-1}$  that could be assigned to carboxylate function as observed in.<sup>[41]</sup> Another possible assignment related to chain degradation<sup>[45]</sup> corresponds to the appearance of C=C bond conjugated to another C=C or C=O.<sup>[43]</sup> The pp-MA spectra of CW, CW x 2 and CW + PW layers seem to be more crosslinked and oxidized, since  $\text{CH}_3$  band at  $1380\text{ cm}^{-1}$  decreases while the C-C and C=O bands at respectively  $1100\text{ cm}^{-1}$  and  $1780\text{ cm}^{-1}$  increase. This phenomenon is emphasized with long duration and thick films (CW x 2 and CW + PW) as observed with the diminution of C=C band  $1630\text{ cm}^{-1}$ . But the oxidation seems to reach a lower degree as OH band increases in case of CW.

After the comparative assignment of each vibration band, the intensity ratio between unsaturated C = C band and CH aliphatic band (CC / CH), between the carbonyl band and CH aliphatic band (CO / CH) was determined (Fig. 3). For all the spectra, band decomposition between  $1855\text{ cm}^{-1}$  and  $1619\text{ cm}^{-1}$  was applied.

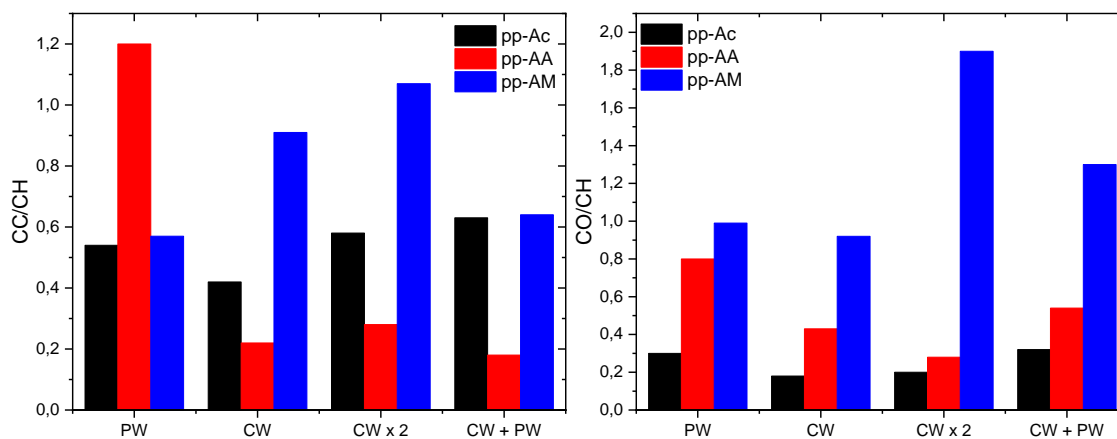
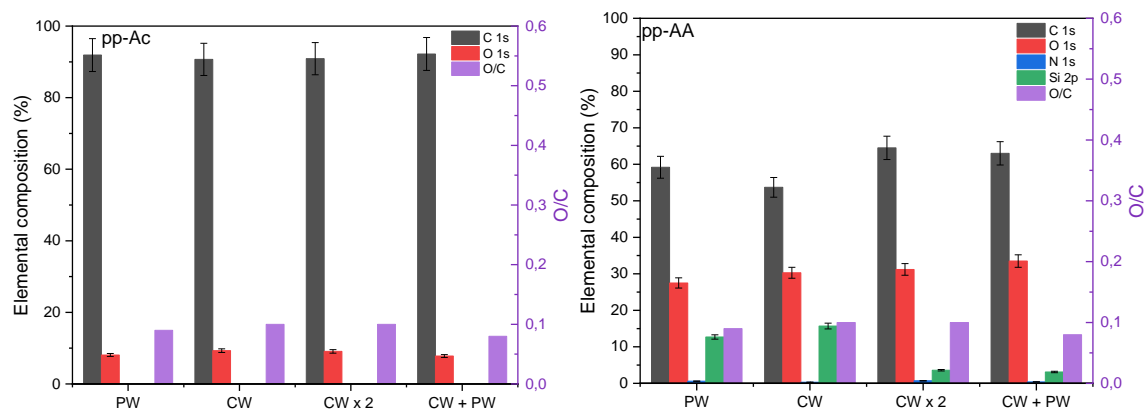


Fig. 3: FTIR ratio (CC / CH and CO / CH) for the different model layers

In case of Ac plasma polymerization, the PW and CW + PW layers present the strongest CO / CH ratio, their chemical structures are therefore more oxidized than the CW and CW x 2. This should be due to a post-oxidation of attached radicals during the plasma deposition. The CC / CH ratios vary from 0.42 up to 0.63. The maximum values come from thicker films coated for longer duration. However, these fluctuations are limited when taking into account the repeatability of the measurements. With pp-AA and pp-MA, these variations are more important. Indeed, in case of pp-AA, the CC / CH ratios are comprised between 0.22 and 1.20. It decreased for thick films, i.e. long plasma duration, and it is more pronounced when the deposition takes place under continuous wave (CW x 2). Its CO / CH ratio, comprised between 0.27 and 0.8 is higher in case of PW and CW + PW, leading to a possible carbonyl retention due to the off time plasma. With pp-MA, the variation of CC / CH and CO / CH ratios respectively from 0.57 to 1.07 and from 0.92 to 1.9 seem to be almost independent on the deposition type. Overall, the FTIR analysis clearly shows the presence of the vibration modes of the characteristic bonds of each precursor and the appearance of new bands in view of PW layer. The semi-quantitative analysis of the ratios does not clearly demonstrate the preservation of the functionalization of the CW + PW and CW x 2 layers when compared to PW and even to the other two layers. XPS analysis makes it possible to differentiate the chemistry of the different layers.

#### Surface chemical composition via XPS spectroscopy

The elementary composition of pp-Ac, pp-AA and pp-MA determined by XPS (raw spectra are given as Fig. S2 in supporting information file) under the various conditions are presented below in the Fig 4.



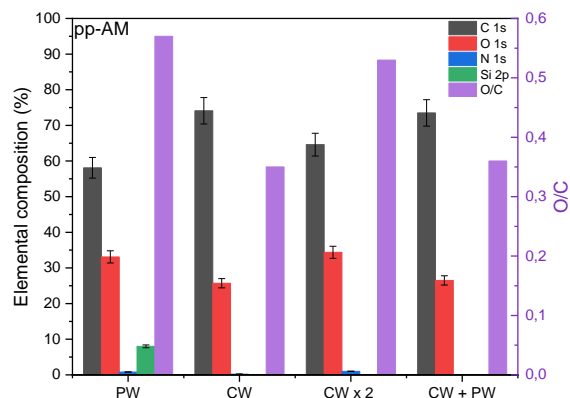


Fig. 4: Elemental composition (XPS, %) of PW, CW, CW x 2 and CW + PW layers (pp-Ac:  $P = 50$  W,  $Q = 40$  sccm, pp-AA and pp-MA:  $P = 10$  W,  $p = 0.01$  mbar)

The broad spectra do not show a great difference in elemental composition according to the mode of synthesis since the XPS spectra of the 4 pp-Ac coatings (Fig. S2, Fig. 4) are similar with peaks assigned to carbon atoms, oxygen atoms in small quantities (8-9%)<sup>[31]</sup> and nitrogen atoms in negligible traces (< 0.2%). The absence of Si 2p and Si 2s peaks shows that the coated layers are thicker than the analyzed depth. Their carbon proportion is greater than 90%.<sup>[44,45]</sup> These high carbon levels indicate that the films are composed mainly of  $sp^2$  and  $sp^3$  carbon bonds.<sup>[6]</sup> The oxygen proportion (8 - 9%) and the O / C ratio of less than 0.1 are low; so the layers are a little oxidized due to free radicals trapped in the polymer layers.<sup>[46,47]</sup>

The broad XPS spectra of the 4 pp-AA layers (Fig. S2, Fig. 4) show the presence of carbon, oxygen atoms, traces of nitrogen and silicon. The appearance of the Si 2p and Si 2s peaks means that the layer thicknesses are less than that the analyzed one, with marked effect for PW and CW (13 - 15 Si %). Their respective thickness is  $\approx 9$  nm and  $\approx 8$  nm (cf Fig. S1). The two other model layer (CW x 2 and CW + PW) spectra show any lower intensity Si peaks explained by thicker films respectively  $\approx 18$  and 15 nm. For all prepared coatings, the carbon content is between 53 and 63% while the oxygen level is important at around 30%. The O / C ratio appears constant, approximately 0.5 for the 4 films, far from the theoretical value equal to 0.75. This deviation is dependent on plasma energy illustrated by the Yasuda ratio ( $W / FM$ )<sup>[7]</sup> and shown in<sup>[48]</sup>. If at first glance, the O / C ratio of the four layers little changes, it must be noticed that this ratio for PW and CW is probably overestimated by the presence of Si-O bonds because of a too low thickness. Only the analysis of high resolution spectra of the carbon peak will allow this ambiguity to be resolved. On the other hand, if we compare only the thickest coatings (CW x 2 and CW + PW), oxidation and therefore stronger functionalization is observed for CW + PW.

The broad XPS spectra of pp-MA coatings (Fig. S2, Fig. 4) also show carbon, oxygen atoms, traces of nitrogen. The presence of peaks of Si 2p, Si 2s at an 8% level is only observed for the deposition in pulsed wave corresponding to a small thickness around 33 nm. The absence of Si peak for the CW layer having an equivalent thickness (30 nm) illustrates in both cases the inhomogeneity of film thickness rather the detection limit of the spectrometer and the resolution limit of the thickness measurement as shown on AFM images (Fig. S3). For the different layers, the carbon content is between 58.1% and 74.1%; the percentage of oxygen varies more significantly compared to other polymers from 25.7 to 34.4%. The O / C ratio varying from 0.35 to 0.57 are higher than those described in <sup>[37]</sup> showing that the capacitive plasma is less degrading than inductively one. However, the same tendency is noticed with the highest value for PW conditions, preserving the initial precursor structure. The value of the O / C ratio of PW as for the pp-AA layers is overestimated due to the possible thickness heterogeneity and the detection of the Si / SiO<sub>2</sub> wafer. Moreover, the chemical structure of pp-MA is dependent on the deposition time, more than on the plasma process. Namely, a long time for the same type of procedure as CW x 2 probably generates thermal heating of the substrate, degradation or / and reorganization of the layer resulting in a stronger oxidation and high O / C ratio. Whereas for CW + PW, more than half of the deposition time (20 min) is devoted to a pulsed deposition for which the electron and ion bombardments are discontinuous.

In order to more accurately determine the chemical structure of each model layer, the decomposition of the C1s high resolution XPS spectra was performed (Fig. 5-10).

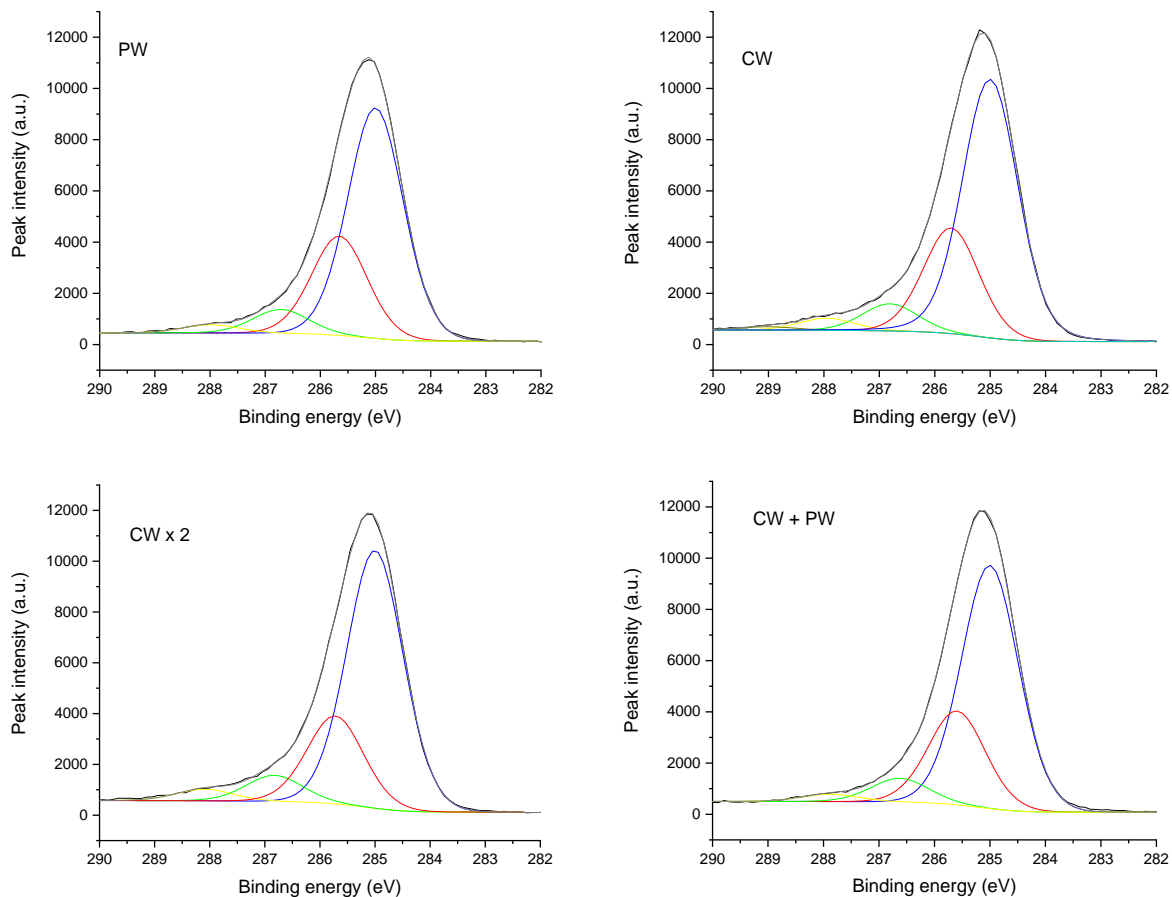


Fig. 5: C 1s high resolution spectra of PW, CW, CW x 2 and CW + PW layers (pp-Ac:  $P = 50$  W,  $Q = 40$  sccm)

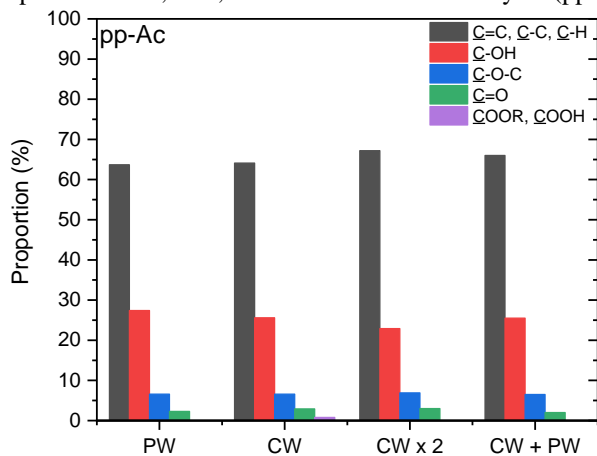


Fig. 6: Assignment and proportion (%) of PW, CW, CW x 2 and CW + PW layers (pp-Ac:  $P = 50$  W,  $Q = 40$  sccm).

The decomposed C 1s spectra with their attribution of each component for the pp-Ac layers are shown in Fig. 5 and 6. The peak shapes of the four layers are similar with the most intense component at 285.0 eV assigned to C-C / C-H and C = C. Indeed, these two substructures are

superimposed. Alcohol groups (C-OH), ether (C-O-C), ketone (C=O) are also identified respectively at 285.8 eV, 286.8 eV, 287.9 eV. Acid or ester groups at 289.0 eV in very low proportion are only detected for CW. The comparison of CW, CW x 2, CW + PW spectra with that one issued from PW layer shows a higher proportion of  $sp^2$  and  $sp^3$  carbon (C-C / CH and C=C) than of oxides (C-OH, C-OC, C=O), specifically for CW x 2. Unfortunately, it is not possible to conclude more deeply about the dependence of the proportion of  $sp^2$  carbon depending on the operating process.

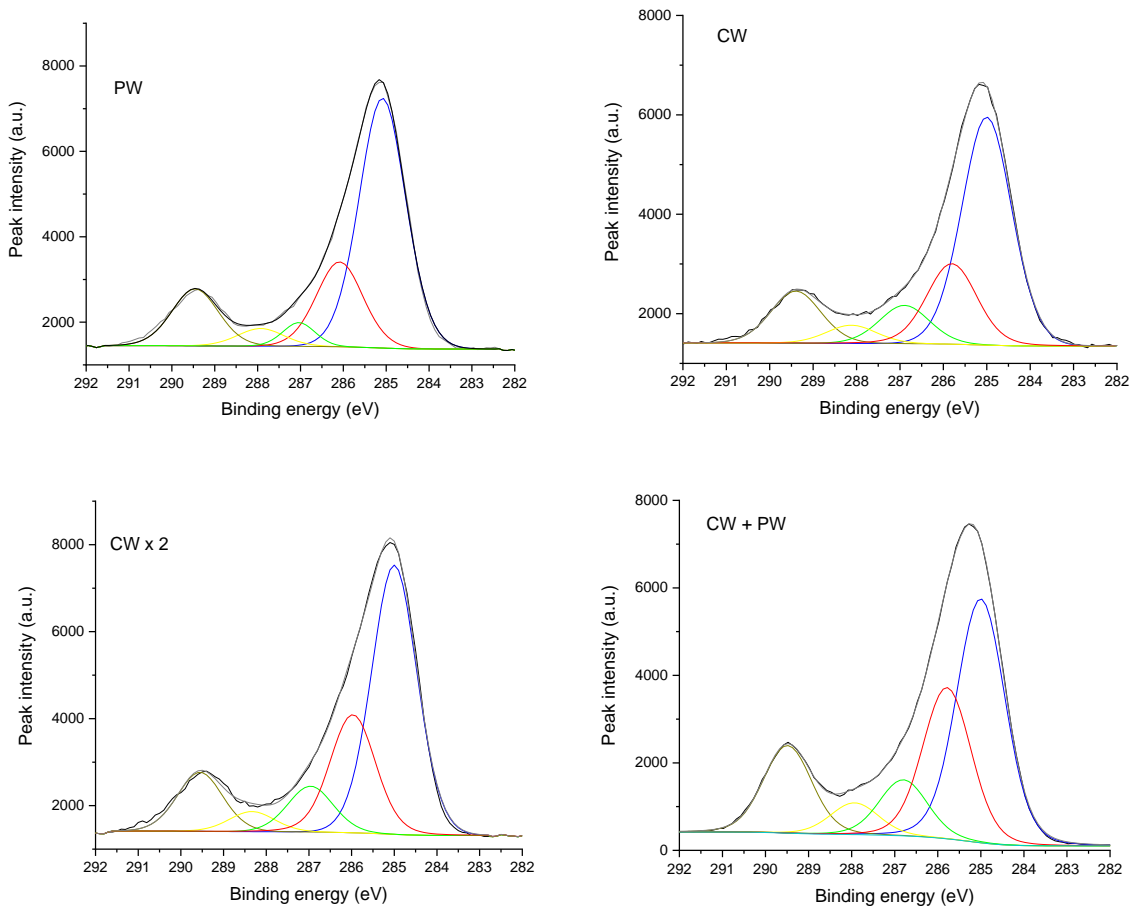


Fig. 7: C 1s high resolution spectra of PW, CW, CW x 2 and CW + PW layers (pp-AA:  $P = 10$  W,  $p = 0.01$  mbar)

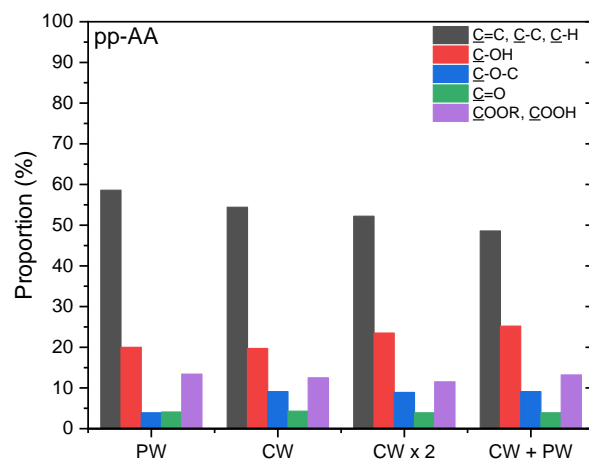


Fig. 8: Assignment and proportion (%) of PW, CW, CW x 2 and CW + PW layers (pp-AA:  $P = 10$  W,  $p = 0.01$  mbar)

The shape of the high resolution spectra for all four layers is similar (Fig. 7,8) with consistent contributions to polyacrylic acid structure. The shift of the maximum peaks  $\pm 0.5$  eV is related to the degree of crosslinking of the polymer. The proportion of C-C/ C-H and C = C bonds decreases from 58.7 % to 48.6 % probably due to the stronger precursor fragmentation in a continuous wave. As regards the variation on the oxygenated groups, only the proportions of C-O-C and COOR change according to the discharge wave. Indeed, the PW layer has the lowest proportion of C-O-C (3.9%); the PW and CW + PW layers have a higher acid concentration (respectively 13.4 and 13.2%) showing thereby little fragmentation of the precursor. These variations confirm those of Pleskunov *et al.* [49] the percentage of the acid and ester groups increases when the duty cycle decreases, that is to say for a higher  $t_{off}$  or a short  $t_{off}$ . As the duty cycle is 100 % for deposits in continuous wave, the percentage of acid / ester is lower compared to coatings in pulsed wave as confirmed by FTIR analysis.

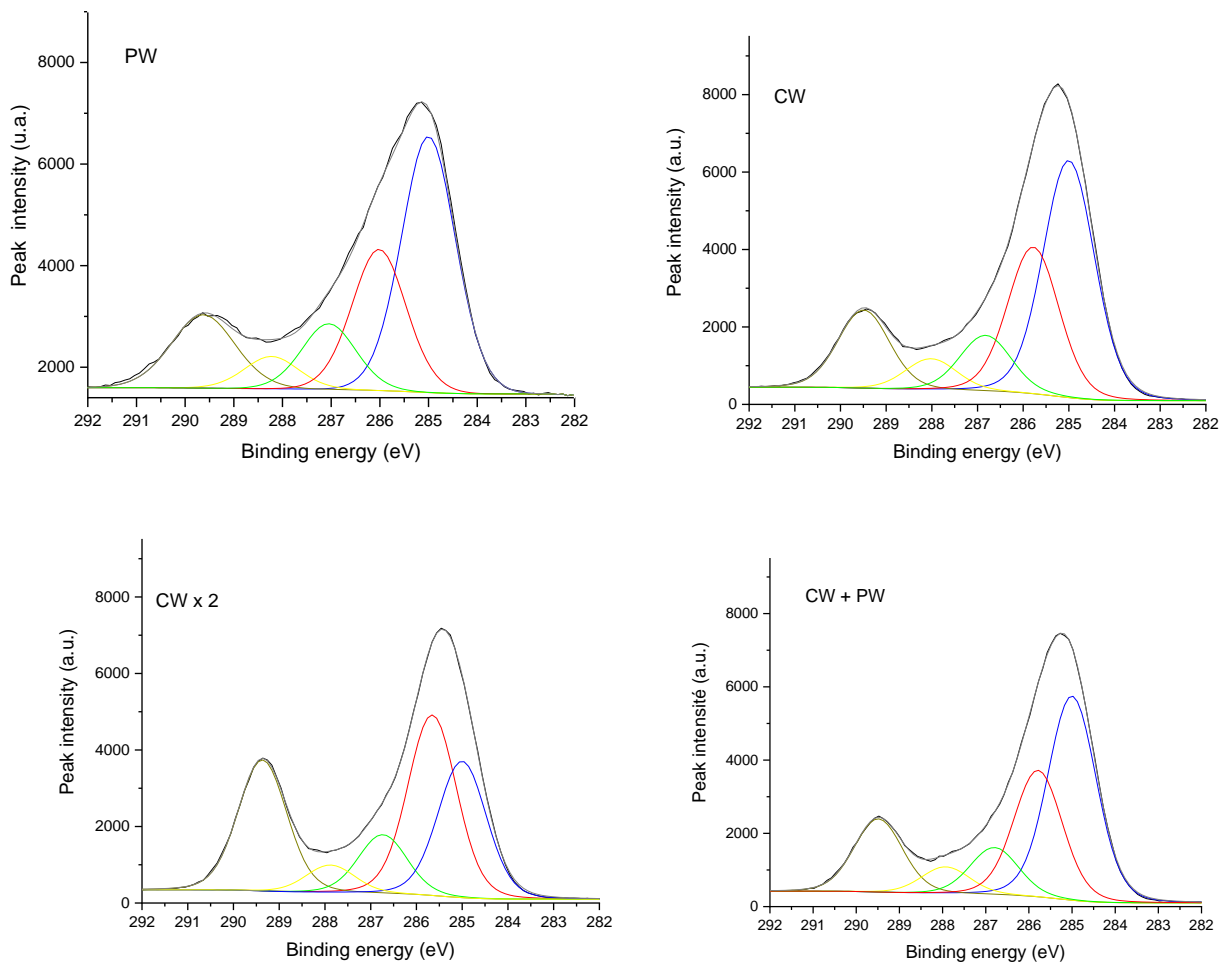


Fig. 9: C 1s high resolution spectra of PW, CW, CW x 2 and CW + PW layers (pp-MA:  $P = 10$  W,  $p = 0.01$  mbar)

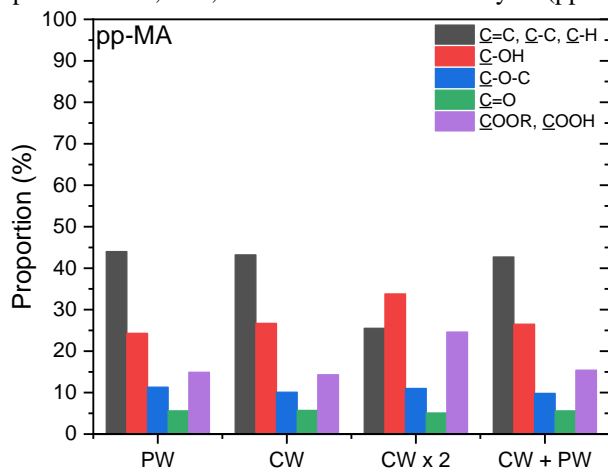


Fig. 10: Assignment and proportion (%) of PW, CW, CW x 2 and CW + PW layers (pp-MA:  $P = 10$  W,  $p = 0.01$  mbar)

Similarly, to pp-AA films, the decomposition of the high resolution C 1s spectra of the four pp-MA is divided into 5 components (Fig. 9,10). With the exception of the CW x 2 layer, the proportions of the different substructures are all of the same order of magnitude. In the case of this layer, the percentage of carboxylic acid and ester is higher (24.4% vs. 14-15%). This should be interpreted as a cleavage of the C = C bonds or of the anhydride rather than anhydride retention as described in the literature for pulsed wave coatings.<sup>[6]</sup>

In summary, the CW, CW x 2 and CW + PW layers from acetylene show a higher proportion of sp<sup>2</sup> and sp<sup>3</sup> carbon (C = C and C - C / CH) than the PW layer. Unfortunately, it is not possible to conclude as to the proportion of sp<sup>2</sup> carbon depending on the process. For acrylic acid, if we compare only the thickest layers (CW x 2 and CW + PW), oxidation and therefore stronger functionalization is observed for CW + PW. Finally, the chemical structure of pp-MA is dependent on the overall deposition time, more than on the wave.

#### *Surface free energy calculated from wetting measurements*

The wetting measurements have the advantage of being more sensitive to surface functionalization compared to XPS spectroscopy. Therefore, the contact angles with water or diiodomethane (WCA or DCA) were determined, followed by the calculation of free surface energies (SFE) and its dispersive and polar components.

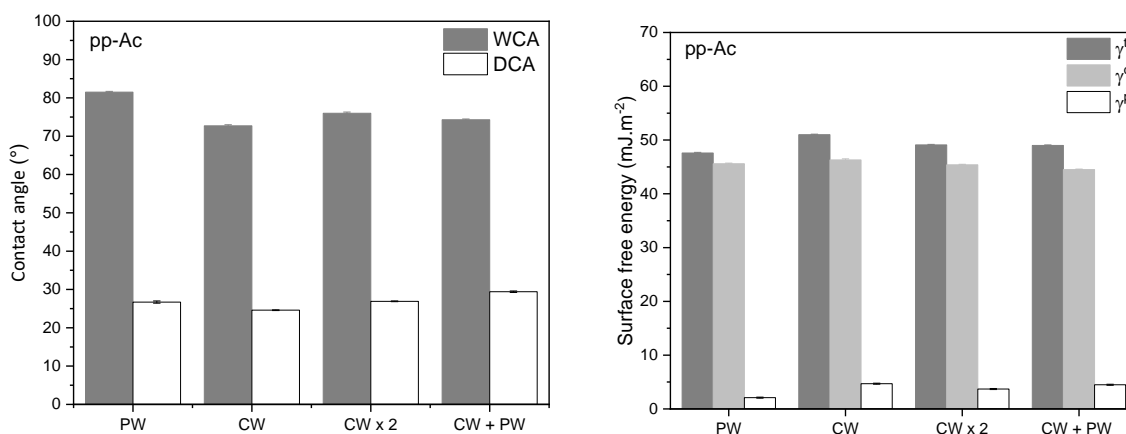


Fig. 11: Contact angles and surface free energies of PW, CW, CW x 2 and CW + PW layers (pp-Ac:  $P = 50$  W,  $Q = 40$  sccm)

This graph (Fig. 11) shows the contact angles with water and diiodomethane of the four pp-Ac layers and the calculated SFE. The contact angles with water are equal to  $81.5 \pm 0.2^\circ$  on PW as also observed in [50],  $72.7 \pm 0.3$  and  $76.0 \pm 0.3^\circ$  respectively on CW and CW x 2, and  $74.3 \pm 0.2^\circ$  for CW + PW. The CW + PW layer is closer to the layers obtained in continuous wave. The PW layer is the most hydrophobic showing the preservation of the hydrocarbon character. DCA variations, even if they are more restricted with the following values  $26.7 \pm 0.3$  for PW,  $24.6 \pm 0.1$  for CW,  $26.9 \pm 0.1$  for CW x 2 and  $29.4 \pm 0.2$  for CW + PW clearly indicate this hydrocarbon character of the PW and CW + PW layers. The associated SFEs and the dispersive component little vary with a difference of  $2.4 \text{ mJ}\cdot\text{m}^{-2}$  for the SFE and  $1.8 \text{ mJ}\cdot\text{m}^{-2}$  for the dispersive term, with nevertheless the lowest value of SFE for the PW layer, a confirmed result with the polar term of  $2.1 \text{ mJ}\cdot\text{m}^{-2}$ , two less important than for the other layers. PW is therefore the most hydrocarbon layer followed by CW x 2, CW + PW and CW.

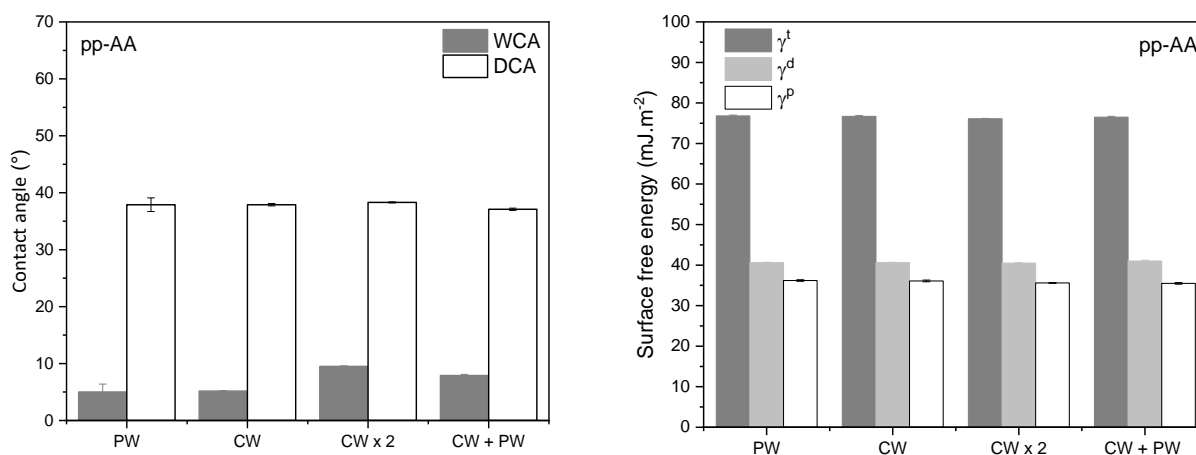


Fig. 12: Contact angles and surface free energies of PW, CW, CW x 2 and CW + PW layers (pp-AA:  $P = 10 \text{ W}$ ,  $p = 0.01 \text{ mbar}$ )

Similarly, WCA and DCA are measured and SFEs calculated for pp-AA (Fig. 12). The contact angles with water for the 4 films are  $5.0 \pm 1.4^\circ$  for PW,  $5.2 \pm 0.1^\circ$  for CW,  $9.5 \pm 0.1^\circ$  for CW x 2 and  $7.9 \pm 0.2^\circ$  for CW + PW. Unlike pp-Ac, the presence of hydrophilic groups such as the acid group allows for a very hydrophilic surface. The lowest value of WCA is obtained for PW whereas the highest value of WCA corresponds to CW x 2. The 2 other layers have intermediate values. These results are in agreement with the results of XPS C 1s high resolution linking well acid concentration and wettability.[51] Conversely, while the coating is carried out in a continuous

wave (CW or CW x 2), the surface becomes more hydrophobic because probably more crosslinked, the plasma phase exhibiting greater densities of precursor fragments. The DCA contact angles are respectively  $37.9 \pm 1.2^\circ$  for PW and  $38.3 \pm 0.1^\circ$  for CWx2 and  $37, 1 \pm 0.2^\circ$  for CW + PW. These DCA results show a surface whose moderately oleophilic character is little dependent on the deposition procedure. The SFEs are all high, between  $76.1 \text{ mJ.m}^{-2}$  to  $76.8 \text{ mJ.m}^{-2}$  and therefore very close to the surface tension of water. The dispersive components vary from  $40.5 \text{ mJ.m}^{-2}$  to  $41 \text{ mJ.m}^{-2}$  and the polar term is between  $35.5 \text{ mJ.m}^{-2}$  and  $36.2 \text{ mJ.m}^{-2}$ . These layers therefore have a wetting behavior close to very hydrophilic surfaces, consequently the theories allowing the calculation of the SFE are limited. For this precursor, the measurement of WCA and DCA is more reliable than the determination of SFE.

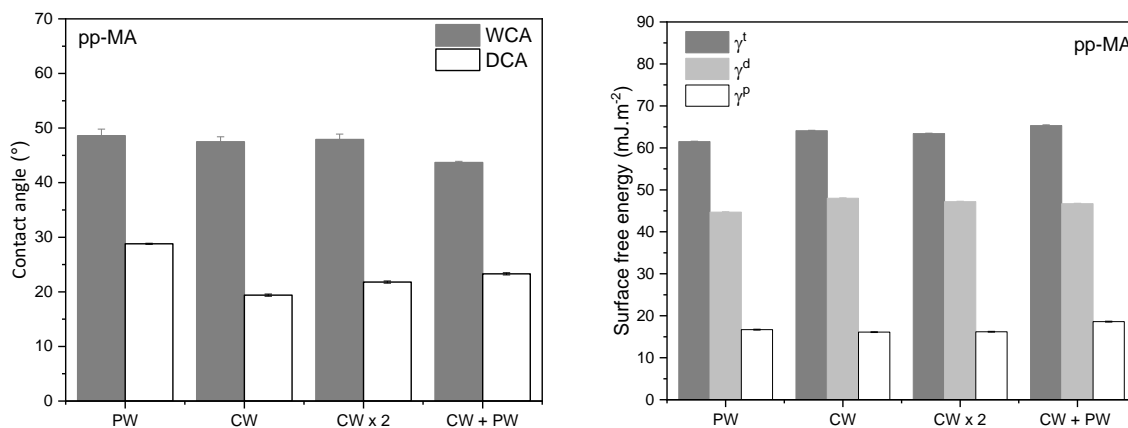


Fig. 13: Contact angles and surface free energies of PW, CW, CW x 2 and CW + PW layers (pp-MA:  $P = 10 \text{ W}$ ,  $p = 0.01 \text{ mbar}$ )

The four pp-MA layers are less hydrophobic than the pp-Ac and less hydrophilic than the pp-AA (Fig. 13). Indeed, the WCA value of PW is  $48.6 \pm 1.2^\circ$ , that of CW  $47.5 \pm 0.9^\circ$ , that of CW x 2  $47.9 \pm 1.0^\circ$  and that of CW + PW  $43.7 \pm 0.2^\circ$ . Alone, the CW + PW layer has a slightly more marked hydrophilic character. Unlike WCAs, DCA values seem to vary a bit more depending on the coating method. The highest value is for deposition in pulsed wave at  $28.8 \pm 0.1^\circ$ . A decrease of  $10^\circ$  was observed for the CW deposition with  $19.4 \pm 0.2^\circ$ . A smaller decrease ( $21.8 \pm 0.2^\circ$ ) is also noted for the CW x 2 deposition. The CW + PW bilayer has an intermediate value at the DCA of PW and CW, namely, and  $23.3 \pm 0.2^\circ$ . This variation of the oleophilic character is to be linked to the deposition procedure with a loss of the chemical functions of the precursor and a more accentuated crosslinking of the layer with the films of CW and CW x 2. The strongest is noted for

the CW + PW layer with  $65.3 \text{ mJ.m}^{-2}$ , the weakest with CW x 2 ( $63.4 \pm 0.2 \text{ mJ.m}^{-2}$ ). The SFE of PW is intermediate although its polar component is higher ( $16.7 \text{ mJ.m}^{-2}$ ) than those of CW and CW x 2 (respectively  $16.1 \text{ mJ.m}^{-2}$  and  $16.7 \text{ mJ.m}^{-2}$ ) but less strong than CW + PW ( $18.6 \text{ mJ.m}^{-2}$ ). The layers synthesized with all or part of a pulsed wave are more hydrophilic and therefore a greater retention of the anhydride function.

In summary, for acetylene, the PW layer is the most hydrophobic showing the preservation of the hydrocarbon character. The CW + PW layer is for its part closer to the layers obtained in continuous wave. With acrylic acid, unlike pp-Ac, the presence of hydrophilic groups such as the acid group makes it possible to have a very hydrophilic or even superhydrophilic surface and therefore only the contact angles need to be taken into consideration. The lowest value of WCA is obtained for PW whereas the highest value of WCA corresponds to CW x 2. The 2 other layers have intermediate values. Finally, the four pp-MA layers are less hydrophobic than those pp-Ac and less hydrophilic than those pp-AA. Alone, the CW + PW layer has a slightly more marked hydrophilic character. The oleophilic character of each of the films is to be linked to the type of frequency chosen (continuous or pulsed) with a loss of the chemical functions of the precursor and a more accentuated crosslinking of the layer with the layers of CW and CW x 2. The layers synthesized with all or part of a pulsed wave are more hydrophilic and therefore a greater retention of the anhydride function.

The adhesion of two materials is strongly dependent on the interfacial energy and consequently on their respective surface free energy. Therefore, the comparative SFE study is one key point for the preparation of cohesive assembly. In comparison with the elastomeric models, adhesion will always be favored for pp-Ac and the least for pp-AA knowing that the NBR and FKM elastomers have  $90.9 \pm 1.2^\circ$  and  $131.2 \pm 3.3^\circ$  with water then  $41.3 \pm 1.5^\circ$  and  $83.9 \pm 7.3^\circ$  with diiodomethane. As observed with WCA values, the polar surface energy increases with the same order: pp-Ac < pp-MA < pp-AA globally from 3 to  $36 \text{ mJ.m}^{-2}$  taking into account the 4 different films. In addition, the surface energies of the two NBR and FKM elastomers have a surface energy of  $39.8 \pm 0.2 \text{ mJ.m}^{-2}$  and  $16.3 \pm 0.6 \text{ mJ.m}^{-2}$ . As there is little difference in surface energy between the 4 layers of each polymer, we therefore expect to have a close bond strength between them for the same given plasma polymer if we consider that the wetting is the most important phenomenon. It has already been discussed that in order to have a strong metal-elastomer assembly at least one surface energy of the elastomer is required which must be close to the surface

energy of the adhesive joint. This explanation leads to a better assembly between pp-Ac and the NBR.

### 3.3 Relevance of the synthesis strategy on the cohesion of a metal / elastomer assembly

In order to prove the efficiency of the adhesive properties with the four model plasma-layers; different assemblies composed of elastomer (FKM or NBR) and metal (stainless steel or aluminum) substrates separated by the plasma coating were prepared as described in the experimental part. After the vulcanization, the assemblies were pulled out using a tack measure.<sup>[52]</sup>

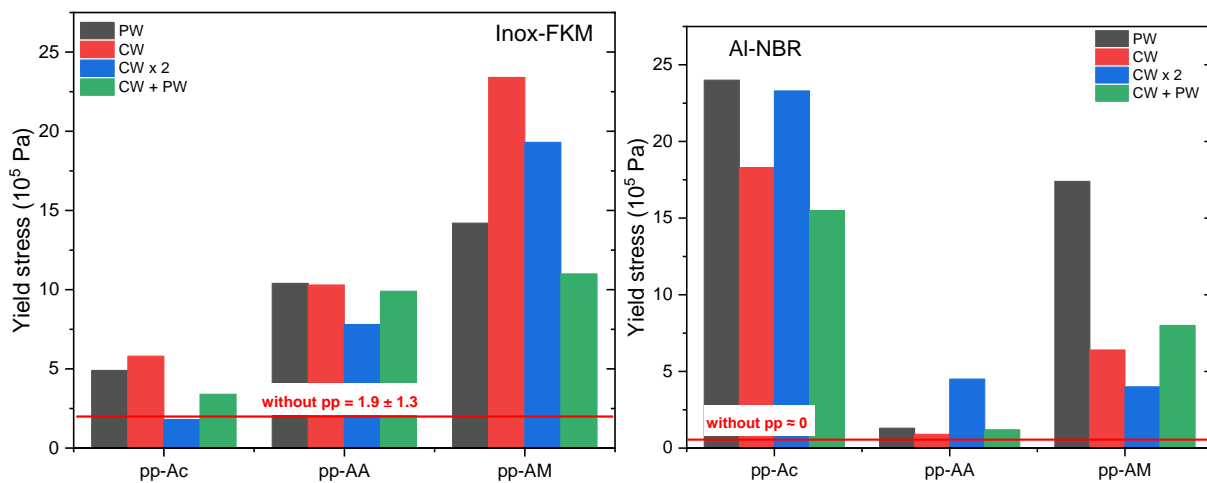


Fig. 14: Yield stress of the different assemblies ( $10^5$  Pa) versus the type of plasma adhesive

Without any plasma layer, the stainless steel - FKM assembly has poor mechanical behavior since its rupture is heterogeneous appearing at low yield stress around  $1.9 \pm 1.4 \cdot 10^5$  Pa. The plasma coating induces, whatever the type of model plasma adhesive, improves the assembly cohesion up to 12 times more compared to the blank assembly. The robustness order of the prepared plasma bond is as follows: pp-MA > pp-AA > pp-Ac. Focusing on the pp-Ac, the yield stress of the 4 layers is comprised between  $1.8 \pm 0.8 \cdot 10^5$  Pa to  $5.8 \pm 1.4 \cdot 10^5$  Pa and lower the thickness is (PW and CW), higher the yield stress is, especially with CW. Thin crosslinked and hydrophobic pp-Ac, as observed for wettability measurements, enhances the fluorinated assembly cohesion. With pp-AA adhesive joint, the thickness and diffusion process do not have great influence while the functionalized and hydrophilic layers (PW and CW + PW, cf XPS analysis) lead to a maximum yield stress even for a hydrophobic and chemically inert material as FKM. However, the yield

stress variation, comprised between  $7.8 * 10^5$  Pa and  $10.4 * 10^5$  Pa for all cases, is weak; therefore, one cannot conclude on a possible chemical anchoring. Pp-MA coating induces an enhancement of yield stress when prepared under continuous wave (CW and CW x 2), this points out the influence of the hydrophobic character as noticed with FTIR spectroscopy (identification of high alkene concentration).

The aluminum – NBR assembly without any plasma joint is completely dissociated after the vulcanization step. Plasma polymers improve the assembly cohesion with the following order: pp-Ac > pp-MA > pp-AA. This result validates the hypothesis on the SFE criterion (cf wettability measure). NBR and pp-Ac are respectively around  $40 \text{ mJ.m}^{-2}$  and  $49 \text{ mJ.m}^{-2}$ . So, closed the plasma polymer SFE is, higher the yield stress is. Beside this thermodynamic adhesion behavior, thickness (diffusion) and functionalization (chemical anchoring) as developed with the four model coatings do not influence the high value of yield stress of this assembly. Pp-AA having the highest value of SFE (around  $76 \text{ mJ.m}^{-2}$ ) do not induce an important increase of the assembly cohesion, except to a lesser extent with CW x 2 layer. With pp-MA, the chemical anchoring due maleic group retention has an effect since the corresponding PW and CW + PW yield stress values are increasing respectively  $17.4 \pm 2.9 * 10^5$  Pa and  $8.0 \pm 2.1 * 10^5$  Pa.

#### 4. Conclusion

The strategy developed here emphasizes either the preservation (or little degradation) of the chemical functions of the precursor, or obtaining of a thick, highly crosslinked layer. This approach also allows a combination of the two effects. The synthesis of these four model layers makes it possible to assess the adhesion mechanisms during the adhesive vulcanization of two different elastomers. For such a goal, the plasma polymerization was carried under pulsed or continuous wave. Kinetic study allows to adjust the total deposition time and the film thickness, the second can vary in the ratio of one to two. The FTIR analysis confirms the chemical function of the PW layers while the XPS interpretation is more dependent on the chemical nature and deposition rate of the precursor. From the SFE determination, it appears that PW pp-Ac is the most hydrophobic while the other layers issued of AA and MA are hydrophilic, even very hydrophilic specially for PW and CW + PW pp-AA. These plasma polymers were applied as adhesive joint for metal - elastomer assemblies and their cohesion was discussed in function of the different adhesion

mechanisms. It appears that the plasma polymer acts as adhesive joint increasing the assembly cohesion, especially with pp-Ac whatever the model layer type even if the other parameters such as chemical anchoring and diffusion may also interfere but in a less proportion.

## **Acknowledgments**

This study is part of the Plasma-Bond project supported by the French agency ANR. The authors wish to acknowledge and to associate the industrial and academic partners of this project; respectively EFJM, Safran.

## **4. References**

- [1] H. K. Yasuda Plasma Polymerization; Academic Press: New York, 1985;
- [2] S. Peter, M. Günther, F. Richter, *Vacuum* **2012**, *86*, 667e671.
- [3] S. Fraser, R. D. Short, D. Barton, J. W. Bradley, *J. Phys. Chem. B* **2002**, *106*, 5596.
- [4] S. A. Voronin, J. W. Bradley, C. Fotea, M. Zelzer, M. R. Alexander, *J. Vac. Sci. Technol.* **2007**, *A 25*, 1093.
- [5] A. T. A. Jenkins, J. Hu, Y. Z. Wang, S. Schiller, R. Foerch, W. Knoll, *Langmuir* **2000**, *16*, 6381.
- [6] S. Schiller, J. Hu, A. T. A. Jenkins, R. B. Timmons, F. S. Sanchez-Estrada R. Foerch, W. Knoll, *Chem. Mater.* **2002**, *14*, 235.
- [7] M. E. Ryan, A. M. Hynes, J. P. S. Badyal. *Chem. Mater.* **1996**, *8*, 37.
- [8] Y. Zhou, B. Rossi, Q. Zhou, L. Hihara, A. Dhinojwala, M. D. Foster, *Langmuir* **2020**, *36*, 837.
- [9] S.A. Visser, C.E. Hewitt, J. Fornalik, G. Braunstein, C. Srividya, S. V. Babu, *Surface and Coatings Technology* **1997**, *96*, 210.
- [10] W. Shen, B. Jiang, S.M. Gasworth, H. Mukamal, *Tribology International* **2001**, *34*, 135-142.
- [11] K. He, Y. Liua, J. Gong, P. Zeng, X. Kong, X.L Yang, C. Yang, Y. Yu, R. Liang, Q. Ou, *Applied Surface Science* **2016**, *382*, 288.
- [12] L. Korner, A. Sonnenfeld, P.R von Rohr, *Plasma Process. Polym.* **2009**, *6*, S660.
- [13] N. Ghali, C. Vivien, B. Mutel, A. Rives, A. *Surf. Coat. Technol.* **2014**, *259*, 504.
- [14] W.B. Liao, Y.C. Chang, Y.A. Lin, H.L. Chen, H.P. Chen, H.S. Wei, C.C.. Kuo. *Thin Solid Films* **2018**, *660*, 678.
- [15] P. Rupper, M. Vandenbossche, L. Bernard, D. Hegemann, M. Heuberger. *Langmuir* **2017**, *33* (9), 2340.

- [16] M. Vandenbossche, D. Hegemann. *Curr. Opin. Solid State Mater. Sci.* **2018**, 22, 26.
- [17] D. Hegemann, E. Lorusso, M.L. Butron-Garcia, N.E. Blanchard, P. Rupper, P. Favia, M. Heuberger, M. Vandenbossche. *Langmuir* **2016**, 32 (3), 651.
- [18] H. Yasuda, T. Hsu, *J. Polym. Sci. Polym. Chem. Ed.* **1977**, 15 (1), 81–97.
- [19] JF. Friedrich, I. Retzko, G. Kühn WES. Unger, A. Lippitz, *Surf. Coat. Technol.* **2001**, 142–144, 460.
- [20] D. Hegemann, E. Körner, S. Guimond, *Plasma Process. Polym.* **2009**, 6 (4), 246.
- [21] J. Drews, H. Launay, CM. Hansen, K. West, S. Hvilsted, P. Kingshott, K. Almdal, *Appl. Surf. Sci.* **2008**, 254 (15), 4720.
- [22] E. Guinter, LC. Fontana, D. Becker, *D. Bull. Mater. Sci.* **2019**, 42 (1), 23.
- [23] M. Ji, A. Jagodar, E. Kovacevic, L. Benyahia, F. Poncin-Epaillard, *Mat. Chem. Phys.* **2021**, 267 12462.
- [24] M. Yatsuzuka, Y. Oka, M. Nishijima, K. Hiraga, *Vacuum* **2008**, 83 (1), 190.
- [25] M.Ebrahimi, F. Mahboubi, MR. Naimi-Jamal, *Diam. Relat. Mater.* **2015**, 52, 32.
- [26] HM.Kang, TH. Yoon, WJ. van Ooij, *J. Adhes. Sci. Technol.* **2006**, 20 (11), 1155.
- [27] P.Rivolo, R. Nisticò, F. Barone, MG. Faga, D. Duraccio, S. Martorana, S. Ricciardi, G. Magnacca, *Mater. Sci. Eng. C* **2016**, 65, 287.
- [28] SA. Evenson, CA. Fail, JPS. Badyal, *Chem. Mater.* **2000**, 12 (10), 3038.
- [29] D.K. Owens, R. C. Wendt, *J. Appl. Polym. Sci.* **1969**, 13, 1741.
- [30] Lide, D. R. *CRC Handbook of Chemistry and Physics, 85th Edition*; CRC Press, 2004
- [31] I. Retzko, J.F. Friedrich, A. Lippitz, W.E.S. Unger, *J. Electron Spectrosc. Relat. Phenom.* **2001**, 121 (1–3), 111.
- [32] A.E. Lefohn, N.M. Mackie, E.R Fisher, *Plasmas and Polymers* **1998**, 3 (4), 197.
- [33] B. Thierry, M. Jasieniak, LCP. de Smet, K. Vasilev, HJ. Griesser, *Langmuir* **2008**, 24 (18), 10187.
- [34] A. Manakhov, L. Zajíčková, M. Eliáš, J. Čechal, J. Polčák, J. Hnilica, S. Bittnerová, D. Nečas, *D. Plasma Processes and Polymers* **2014**, 11 (6), 532.
- [35] D.O.H.Teare, W.C.E. Schofield, V. Roucoules, J.P.S. Badyal, J. P. S. *Langmuir* **2003**, 19 (6), 2398.
- [36] G. Mishra, S.L. McArthur. *Langmuir* **2010**, 26 (12), 9645.

- [37] F. Siffer, A. Ponche, P. Fioux, J. Schultz, J. Roucoules, V. Analytica Chimica Acta **2005**, 539 (1), 289.
- [38] M. Hesse, H. Meier, B. Zeeh, *Spectroscopic Methods in Organic Chemistry*, 2nd ed.; Georg Thieme Verlag: Stuttgart, **2008**; b-003-108602.
- [39] K. Ichihara, T. Kawai, M. Kaji, MA. Noda, Agr. Bio. Chem. **1976**, 40(2), 353.
- [40] E. Kasparek, J. R. Tavares, M. R. Wertheimer, P-L. Girard-Lauriault. Langmuir **2018**, 34, 12234.
- [41] MR. Alexander, S. Payan, TM. Duc, Surface and Interface Analysis **1998**, 26 (13), 961–973.
- [42] A. Larrañaga, S. Petisco, R. Villanueva, JJ. Iturri, S. Moya, E. Meaurio, JR. Sarasua, European Technical Conference-Society of Plastic Engineers; 2011.
- [43] G. Socrates. Journal of the American Chemical Society **1995**, 117 (5), 1671.
- [44] G. Le Dû, N. Celini, F. Bergaya, F. Poncin-Epaillard, Surf. Coat. Technol. **2007**, 201 (12), 5815.
- [45] J. Friedrich, R. Mix, G. Kühn, I. Retzko, A. Schönhals, W Unger, Composite Interfaces **2003**, 10 (2–3), 173.
- [46] J. Kieser, M. Neusch. *Thin Solid Films* **1984**, 118 (2), 203.
- [47] H. Yasuda, M.O. Bumgarner, H.C. Marsh, N. Morosoff, N. *J. Polym. Sci. Polym. Chem. Ed.* **1976**, 14 (1), 195.
- [48] A. Fahmy, TA. Mohamed, A. Schönhals, Plasma Chem Plasma Process **2015**, 35 (2), 303.
- [49] P. Pleskunov, D. Nikitin, R. Tafichuk, A. Shelemin, J. Hanuš, I. Khalakhan, A. Choukourov, A. The Journal of Physical Chemistry B **2018**, 10.1021.
- [50] M. Samadi, A. Eshaghi, SR. Bakhshi, AA. Aghaei, Opt Quant Electron **2018**, 50 (4), 193.
- [51] M. Tatoulian, F. Arefi-Khonsari, JP. Borra, Plasma Processes and Polymers **2007**, 4 (4), 360.
- [52] GR. Hamed, Rubber Chemistry and Technology **1981**, 54 (3), 576.

## Table of contents

This paper deals with the synthesis of model plasma layers for the preparation metal – polymer assembly. Four layers were developed using combinations of pulsed and continuous wave and characterized in order to determine the chemical retention, surface energy and thickness related to adhesion mechanism. Finally, illustration is given on the cohesion of metal – elastomer assembly.

## Graphic

